Novel methods for shaping thin-foil optics for x-ray astronomy

Ralf K. Heilmann[a], Glen P. Monnelly[a], Olivier Mongrard[a], Nat Butler[a], Carl G. Chen[a], Lester M. Cohen[b], Christopher C. Cook[c], Lee M. Goldman[d], Paul T. Konkola[a], Mike McGuirk[a], George R. Ricker[a], and Mark L. Schattenburg[a]

[a] Center for Space Research, Massachusetts Institute of Technology, Cambridge, MA 02139, USA
[b] Smithsonian Astrophysical Observatory, Cambridge, MA 02138, USA
[c] Axsun Technologies, Billerica, MA 01821, USA
[d] Raytheon Lexington Laboratory, Lexington, MA 02421, USA

ABSTRACT

We report on progress in developing low-cost methods for shaping thin-foil glass x-ray optics. Such optics might serve as substrates for reflection gratings or as foil mirrors in high-throughput missions such as Constellation-X. Novel thermal shaping to lithographically defined pin chucks leads to the desired shape with high accuracy, thereby avoiding the need for replication. To demonstrate this method we have produced 200 micron-thick glass sheets with sub-micron flatness and half power diameter below 10 arc seconds. We also present a process for depositing low-stress metallic coatings that provides high x-ray reflectivity without significant foil distortion.

Keywords: X-ray telescopes, thin-foil x-ray optics, Constellation-X, thermal shaping, slumping, pin chuck, low-stress coating

1. INTRODUCTION

Since its launch in 1999, the Chandra x-ray telescope has delivered x-ray images of the universe with unprecedented resolution.[1,2] However, its arc second angular resolution was only possible due to its very expensive monolithic mirror design with a poor collecting-area-to-mass ratio of about 10^{-4} m^2/kg. The segmented x-ray foil-optic approach followed in the ASTRO-E design achieved a ratio improvement of more than an order of magnitude, but was limited to arc minute angular resolution. For future instruments such as the Constellation-X Spectroscopy X-ray Telescope (SXT) a combination of large effective collecting area (≈ 0.4 m^2 per mirror), low mass (< 400 kg), and high resolution (< 15 arc seconds half power diameter (HPD)) is desired.

Over the last few years much progress has been made in the shaping and accurate mounting of the thin foils that provide the reflecting mirror surfaces.[3–8] Inexpensive glass microsheets, mass-produced in the flat panel display industry, serve as the foil material of choice due to their strength, low density, relative flatness and homogeneity, and smoothness on sub-mm length scales. The glass sheets are thermally formed to either concave[7] or convex[8] mandrels with radii of curvature in the tens of centimeters appropriate for Wolter I type designs. Overall figure values for individual glass sheets as low as 10 arc seconds (after replication) have been reported,[8] as well as about 30–35 arc second HPD for reflector pairs[8] and single-bounce multi-shell prototype mirrors.[7]

While the use of glass foils for Wolter I type x-ray mirrors promises a very attractive combination of high throughput, low mass, and good resolution, the same approach has not yet been pursued for the building of x-ray reflection gratings. For example, about half the collecting area of the Constellation-X SXT is to be covered by lightweight high-efficiency reflection gratings.[9,10] Conventional grating fabrication techniques, employing replication from ruled masters and mechanical thinning of substrates as in the case of the XMM gratings, currently cannot achieve the combination of flatness, stiffness, low weight, and high efficiency required for the Constellation-X mission. If they can be formed well enough, microsheets could reduce the weight of reflection gratings by a factor of 3–6 compared to XMM. Apart from reflection gratings, flat glass microsheets could also find application as mirrors in Kirkpatrick-Baez (KB) type x-ray telescope designs,[11] where the ideal mirror shape is very close to being perfectly flat.

Further author information: (Send correspondence to R.K.H.)
R.K.H.: E-mail: ralf@space.mit.edu

X-Ray Optics for Astronomy: Telescopes, Multilayers, Spectrometers, and Missions, Paul Gorenstein, Richard B. Hoover, Editors, Proceedings of SPIE Vol. 4496 (2002) © 2002 SPIE · 0277-786X/02/$15.00

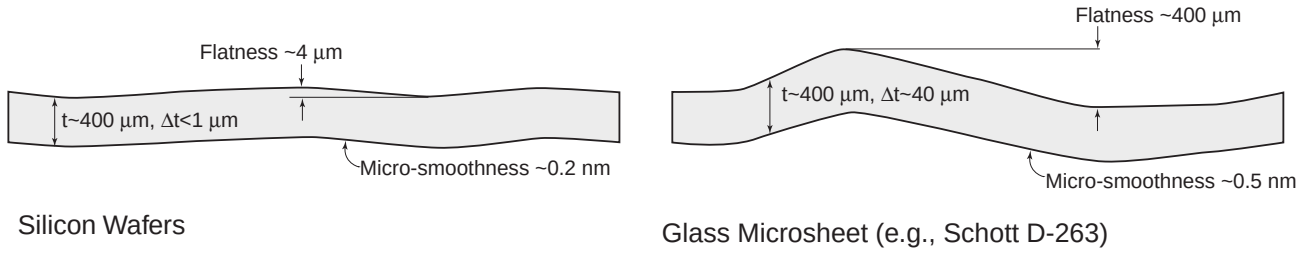

Figure 1. Schematic comparison of substrate properties of Si wafers and glass microsheets. The vertical scale is greatly exaggerated for clarity.

We have previously developed the technology to manufacture super-smooth gratings on precisely miscut Si wafers[12] and propose to transfer the grating profile via nanoimprint lithography onto glass foils that have been thermally shaped to a flat surface.

In this paper, we describe our results on the use of flat mandrels and novel techniques to thermally shape glass microsheets to a high degree of flatness. Based on our experience with dust particle contamination, we manufactured lithographically-defined pin chuck mandrels that minimize the contact area between glass and mandrel as well as print-through from dust particles. An anti-stick coating prevents fusing to the pins during slumping. We achieve as little as 10 arc second rms angular deviation over a several cm^2 sized area.

After shaping, these foils generally have to be covered with a metal coating to improve their reflectivity at x-ray wavelengths. Such coatings often induce stress on the substrate that can lead to significant bowing over the size of a 10–20 cm thin-foil optic. In Section 4 we describe how that bowing can be kept at the sub-micron level through low-stress double-sided coating.

2. SUBSTRATE PROPERTIES

The substrates that carry reflection gratings should be light-weight, mechanically strong, macroscopically flat, and microscopically smooth. High-efficiency blazed reflection gratings with nearly atomic smoothness on the grating facets can be produced by interference lithography on graze-cut Si(111) wafers.[12] Commercially available Si wafers posses very low roughness (on the order of tenths of nanometers) and thickness uniformity (typically better than ± 1 μm for a thickness of about 400 μm), but the flatness of a 100 mm diameter wafer is limited to 2–7 μm due to the imperfect slicing process[13] (see Fig. 1). This is not a problem in the semiconductor industry, where wafers are often held flat on vacuum chucks during processing, but it is unacceptable for a SXT reflection grating. We are also currently investigating methods to flatten Si wafers to the sub-micron level.

In comparison, glass microsheets, such as Schott D-263 or AF-45, have sub-nanometer roughness, vary in thickness over a few microns per centimeter along the surface, and have a figure that can easily exceed their thickness for 200 μm-thick sheets of 10×10 cm^2 (see Fig. 1). However, due to the amorphous structure of glass the low-spatial frequency figure can be vastly improved through thermal shaping, i.e. slumping. Furthermore, glass can be slumped to surfaces with rather small radii of curvature.[3–5,7,8]

If the slumping process produces thin glass sheets of sufficient flatness and smoothness on length scales from tens of centimeters (figure) to sub-nanometers (roughness) a conformal grating structure could be added to the glass through a "squish and flash" nanoimprint lithography replication technique, utilizing a high-efficiency Si grating master manufactured according to Franke *et al.*,[12] and fast backside UV curing of epoxy[14] (see Fig. 2).

3. GLASS SHAPING RESULTS

We use 200 μm thick Schott D-263 borosilicate glass in all our experiments. Thermal shaping takes place inside a copper box (which maintains good temperature uniformity) that is placed inside a commercial oven. The experiments are performed inside a class 100 cleanroom.

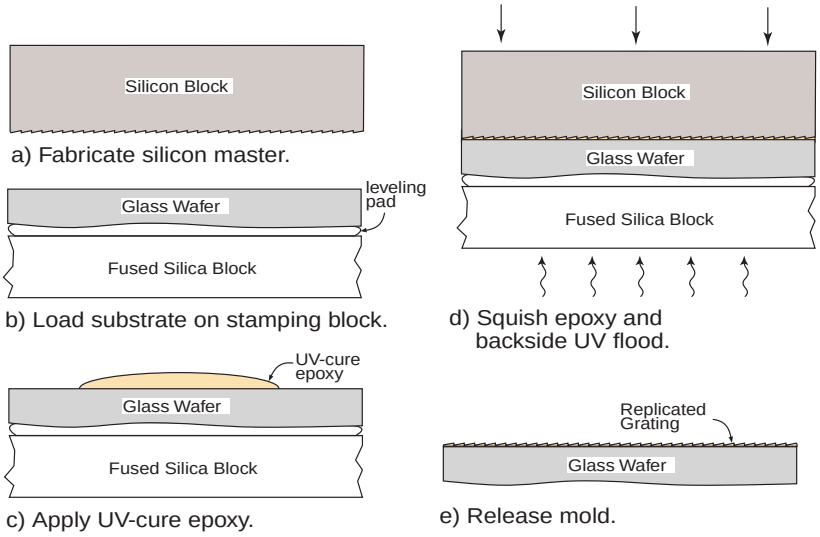

Figure 2. Grating replication sequence. The Si master is thick enough to be polished flat before the master grating is generated. The grating pattern is replicated into a thin layer of UV curable epoxy (cure time on the order of a few seconds or less) on the face of a glass sheet that has previously been slumped to a flat mandrel.

3.1. Dust particle contamination

Initially we tried to slump 200 μm thick 50×50 mm^2 microsheets to an optical flat without particular cleanliness precautions by gradually heating up the flat with a sheet on top to 610 ^{o}C, followed by a slow cool down. As shown in Figs. 3 (a)–(b) the sheet flatness typically improved from $\sim$ 100 μm to $\sim$ 5 μm, as measured by an in-house surface metrology tool based on the Hartmann test[15] (see Fig. 4). We generally observe edge effects, especially at corners, which manifest themselves as sharp bends up to 10 μm in height. These effects might be reduced through elimination of defects such as cracks or fissures along the edges before slumping, or by slumping oversized sheets and cutting them afterwards.

Also visible in the Hartmann data in Fig. 3 (b) are many small bumps 1–5 μm in height and around 5–10 mm in diameter. We experimentally determined these deformations to be due to μm size dust particles on the mandrel that print through the slumped glass sheet. RCA cleaning[16] both mandrel and glass sheet before slumping greatly reduces the number of dust particles enclosed between the two parts. However, during slumping of clean parts optical contact bonding takes place, and the glass sheets shatter due to the mismatch in thermal expansion coefficient between glass and mandrel. We therefore concluded that the presence of dust particles is actually essential to the success of slumping to a smooth mandrel, since it prevents direct contact between parts.

In previous work on the shaping of curved thin-foil glass optics mainly two different approaches have been followed. In one approach the microsheets are first slumped to a convex mandrel. This process probably leads to deformations due to dust particles similar to what we observe. Then a separate, precisely polished convex mandrel is coated with a thin gold film. Mandrel and formed glass sheet are joined under vacuum with an intermediate, several μm thick epoxy layer. After epoxy curing the two parts are separated mechanically. Separation occurs at the weakly adhering gold/mandrel interface, so that the smooth mandrel surface is replicated onto the now gold covered glass sheet.[5,8] The epoxy layer is probably thick enough to cover most left-over dust particles and to smooth out contamination related deformations without detrimental effects on the smoothness of the final gold/epoxy covered glass substrate. However, epoxy replication adds several expensive and time-consuming steps to the manufacturing process and leaves the foils with an elastic, somewhat unstable epoxy layer that might continue to change over long time scales. Bimaterial bending due to epoxy shrinking also has to be considered.[17]

In the other approach microsheets are slumped onto a concave quartz mandrel, sometimes separated by a Si cloth.[4,18] The side of the glass sheet that is not in contact with the mandrel is then coated with a graded multilayer to provide optimized reflectivity in the hard x-ray band.[19] For this configuration dust particles could either be

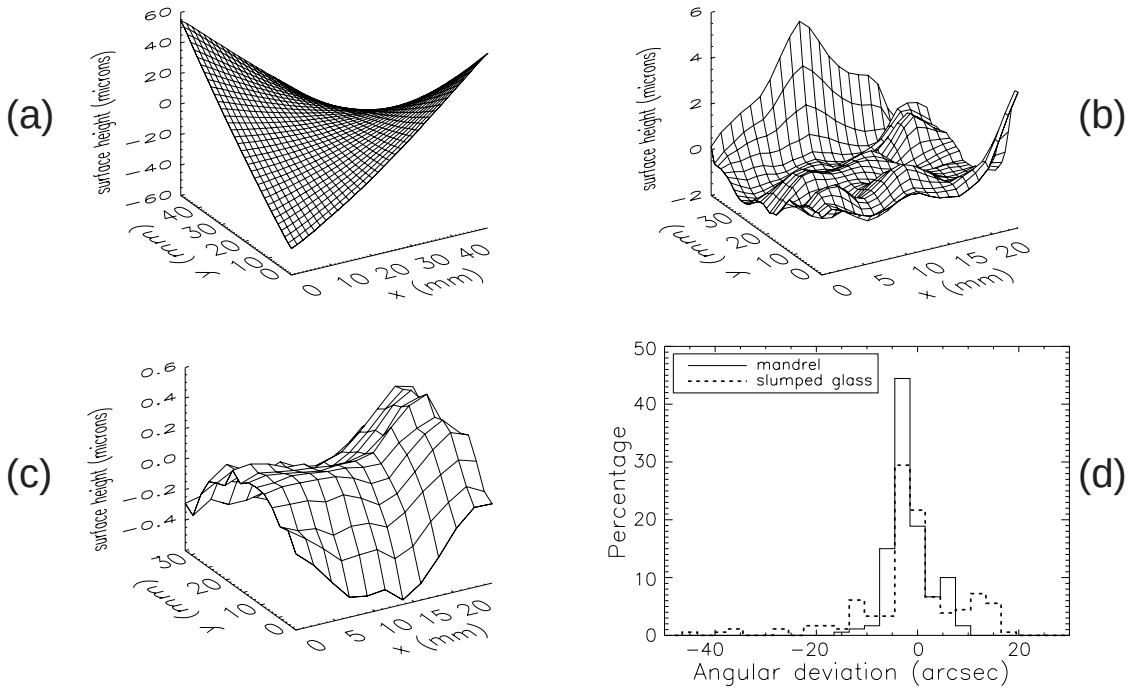

Figure 3. Hartmann topographs from 50×50 mm^2 glass sheets. (a) shows data from an unslumped sheet, (b) from a sheet after slumping to a flat mandrel, and (c) from a sheet after slumping to a non-sticking pin chuck. (d) shows a histogram of angular deviation for the pin chuck (solid line, rms = 4 arc seconds) and for the data from (c) (dashed line, rms = 10 arc seconds, HPD = 5.9 arc seconds). In (b) and (c) the edges have been omitted. Note the 100× change in vertical scale from (a) to (c).

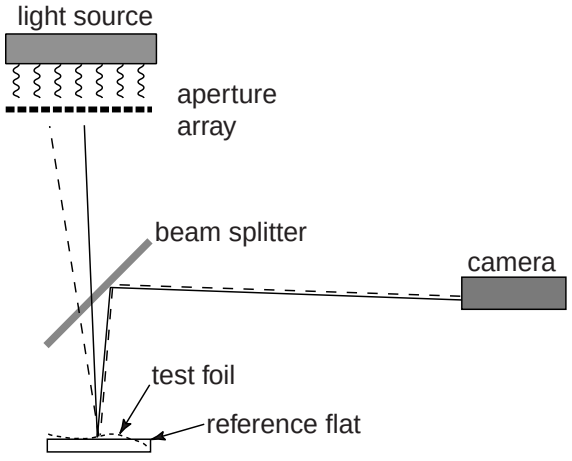

Figure 4. Schematic of Hartmann foil surface metrology measurement tool. A grid of light sources is reflected from the test optic and imaged onto a CCD. The test surface topography can be deduced from the deviation of the grid image from that of a flat reference.

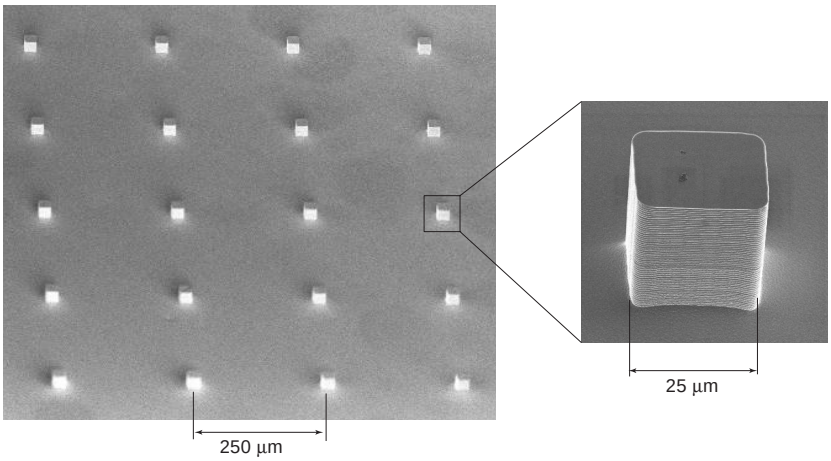

Figure 5. Scanning electron micrograph of a silicon pin chuck.

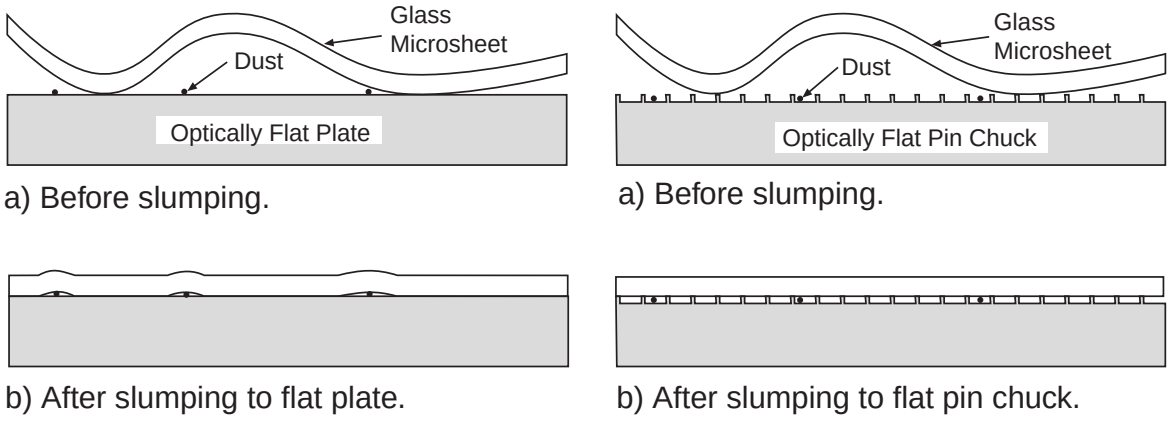

Figure 6. Thermal shaping of glass microsheets. Left: Slumping to flat mandrel. Trapped dust particles can lead to deformations on both sides of a thin glass sheet. Right: Slumping to pin chuck. Most dust particles that are smaller than the pin height will be located between the widely spaced pins and have no contact with the glass sheet. The macroscopically short distance between pins prevents the glass to sag noticeably in the space between them.

integrated into the Si cloth, or possible print-through could affect the figure at spatial frequencies on the order of cm^{-1}. Interestingly, when contact between mandrel and microsheet is limited to the edges of the sheet ("free-forming") the best slumping results are obtained, and the formation of ripples with wavelength ~ 2 cm is avoided.[18]

3.2. Shaping to pin chucks

In order to minimize deformation caused by dust particles trapped between mandrel and glass sheet we followed a different approach. We first lithographically manufactured a flat silicon pin chuck with thousands of ~ 25 μm high and 25×25 $\mu\mathrm{m}^2$ wide pins arranged in a 250 μm period square grid pattern (see Fig. 5). Lithography and processing were similar to the steps described by Chen *et al.*[20]

As illustrated in Fig. 6 the underlying idea is that the space between the pins is deep enough to take up micron sized dust particles and prevent them from deforming the glass, which leads to a ~ 100 times smaller probability of trapping dust between the parts, while at the same time the surface contact area between glass sheets and mandrel is greatly reduced.

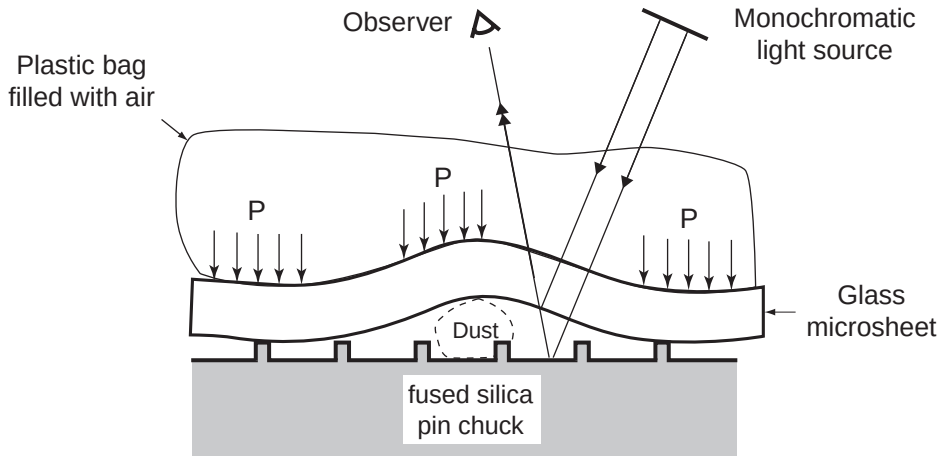

Figure 7. Schematic of the bag test. A plastic bag filled with air is used to apply a uniform pressure against the glass sheet. If a dust particle prevents the sheet from flattening to the top of the pins the resulting wedge between the bottom of the glass and the mandrel surface will produce concentric interference fringes.

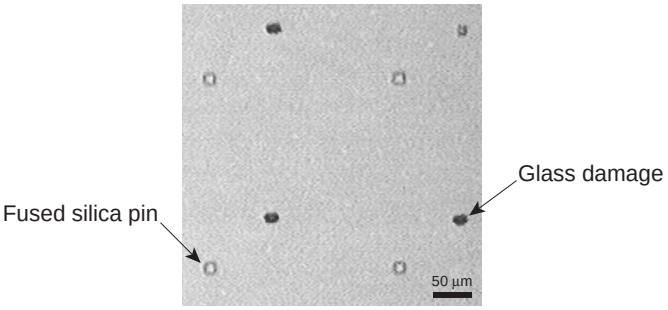

Figure 8. Microscope view of a slumped glass sheet on top of a TiO_2 coated fused silica pin chuck (pin roughness < 1 nm), focused through the glass onto the pins. The glass sheet has been translated slightly to reveal the damage from contact with the pins. No such damage is observed when slumping to a mandrel with a coating of > 5 nm roughness.

While lithographic processing on Si is straightforward, fused silica is easier to work with and to figure for use as a shaping mandrel. We therefore subsequently produced fused silica pin chucks with the same pin pattern. The processing starts with a $\sim 100 \times 100 \times 2.3$ mm^3 fused silica photomask, coated with Cr and resist, that is exposed through a mask containing the pin pattern, and followed by development, chrome etching, and HF etching. The last step limits the etch depth to < 5 μm, since the wet etch leads to undercutting of the Cr/resist covered pins. After stripping of the remaining resist and Cr the typical pin size has shrunk to $\sim 15 \times 15 \times 3$ μm^3.

Slumping to the fused silica pin chuck gives much fewer deformations that can be traced to dust particles. However, despite RCA cleaning, occasionally there are still larger dust particles caught between microsheet and mandrel. To ensure successful slumping we inspect each mandrel/microsheet pair at room temperature before slumping with a bag test (see Fig. 7). This test gives a good indication of the glass shape after slumping and allows detection of trapped particles that can lead to undesired deformations. Once such a particle is localized it can usually be removed through concentrated blasts with a CO_2 snow gun. However, even with the bag test inside the cleanroom it is difficult to achieve less than $\sim$ one visible particle per 10 cm^2.

Even if the bag test shows no trapped contamination and promises a good slumping result the glass can still be damaged in the shaping process. In several experiments occasional fusing between the glass and a pin led to either breaking of a pin or loss of a small piece of glass that remained stuck to a pin. We believe that contact bonding to

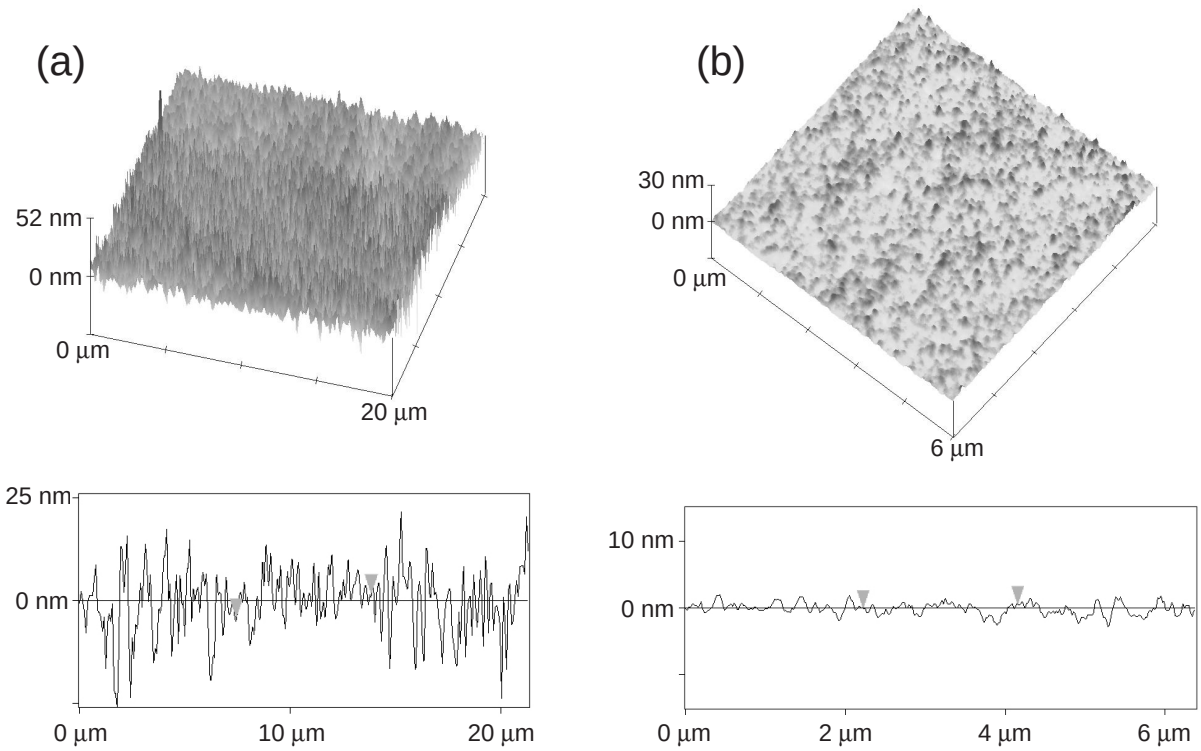

Figure 9. Atomic force microscopy data of two TiO_2 coated fused silica mandrels. For each mandrel, a 3D plot of the measured surface is given along with a height profile. The data in (a) is from a non-sticking mandrel (rms roughness = 5.1 nm), and (b) from a sticking mandrel (roughness = 0.7 nm).

the pins increases friction that prevents the glass from expanding and contracting freely relative to the mandrel, and once it sticks to the top of a pin for some time at high temperatures the probability for fusing increases dramatically.

Subsequently we covered the mandrel with a 2-3 μm thick, rough layer of TiO_2 through e-beam evaporation (at MIT Lincoln Laboratory) to prevent fusing. The roughness of this "anti-stick" layer is found to be the key to a useful shaping mandrel. If the roughness is too small the slumping results do not improve (see Fig. 8), while for large roughness ($\approx$ 5 nm) no damage to glass or mandrel is observed (see Fig. 9). In the latter case the central portion of a 50×50 mm^2 glass sheet shows rms surface height variations of 0.2 μm, an rms surface angular deviation of 10 arc seconds, and a HPD of $\sim$ 6 arc seconds (see Fig. 3(c)).

In Fig. 3(d) the histogram of angular deviation is shown for the mandrel and the slumped sheet from Fig. 3(c). The rms angular deviation for an optical flat is comparable to the value obtained for the mandrel and indicates the measurement accuracy of our Hartmann system. The 10 arc second value for the slumped microsheet is therefore an upper limit on its rms surface angular deviation.

The measurement accuracy of glass sheet topography is currently limited since at the wavelengths of visible light a non-negligible percentage of the light is reflected from the back surface of the microsheets. Repeated surface height measurements of the same sheet agree to a level of $\sim$ 0.2 μm, and the lateral resolution is about 2 mm. Large improvements in accuracy, repeatability and resolution are expected from a future Shack-Hartmann wavefront sensor that operates at deep UV wavelengths and which is described by McGuirk *et al.*[21]

The measurement system shown in Fig. 4 is not sensitive on the scale of the 250 μm period of the pins on the mandrel. We therefore measured a slumped sheet, covered with a reflective 70 nm Al layer, with a Wyko interferometer with a nominal lateral resolution of 3 μm and vertical resolution of 0.3 nm. To the level of $\sim$ 2–3 nm no evidence was found for any sagging or impressions that could arise from the fact that the microsheet rests on a periodic structure during shaping.

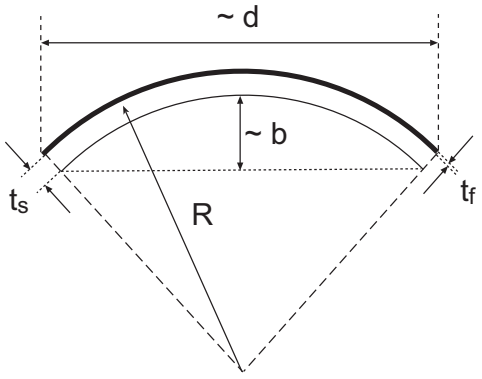

Figure 10. Schematic of a flat substrate, deformed to radius R by stress due to the deposited thin film.

4. LOW-STRESS COATINGS

In general when a thin film of one material is applied to a substrate of a different composition compressive or tensile stress arises that leads to deformation or bending of the substrate. The relationship between the average thin-film stress σ and the radius of curvature R of a substrate that was flat before film deposition is given in its simplest form by the Stoney equation[22]

$$\sigma = \frac{E}{(1-\nu)}\frac{t_s^2}{6Rt_f} = \frac{4}{3}\frac{E}{(1-\nu)}\frac{t_s^2 b}{t_f d^2}, \tag{1}$$

where $E/(1-\nu)$ is the biaxial elastic modulus of the substrate, t_s and t_f are the substrate and film thicknesses, respectively, b is the bending height or bow, and d is the diameter of a circular substrate. For example a 200 μm thick glass sheet ($E/(1-\nu) = 9.2 \times 10^{10}$ Pa for D-263) of diameter 20 cm covered with a 25 nm thick film with $\sigma = 300$ MPa would bow by 60 μm, which corresponds to an angular deviation > 4 arc minutes at the edge.

Large-area thin foils for x-ray optics should assume their ideal shape as closely as possible without any external applied forces. In this way, mounting forces that might introduce additional foil deformation can be minimized and overconstraints can be avoided.[6,23] For example, if a glass sheet has been thermally formed as described above to a flat as the ideal shape, then deformations through subsequent processing steps should be kept to a minimum. However, to achieve reasonable x-ray reflectivity in the sub-10 keV range at practical angles of incidence a reflective coating such as gold is applied, which can cause substrate bending due to thin film stress. Of course the same argument applies if thin Si wafers are used as substrates.

Intuitively one way to compensate for thin film stress is simply to coat both sides of a substrate with the same film. We tested this idea on thin Si wafers first, since for glass substrates reflection from the back surface can compromise accurate measurements.

4.1. Evaporated Cr/Au films

We measured the bow of ~ 400 μm thick, 10 cm diameter, double sided polished Si(100) wafers with a Tencor FLX 2320 thin film stress measurement apparatus. This instrument scans a laser beam along a straight line across the wafer surface and deduces the local surface slope from the position of the reflected beam. The curvature $1/R$ is obtained by linear regression from a graph of slope versus distance along the surface. The bow b is the maximum height deviation from planarity along the measured line. Values for b were typically in the range of 2–7 μm.

The wafers were then coated with a 5.0 nm buffer layer of Cr and a 20.0 nm layer of Au. The layers were deposited at a rate of 0.5 nm/sec. Four wafers were coated on one side only, and five were covered on both sides. The results did not differ significantly whether deposition took place in a stationary e-beam evaporator or in a planetary evaporator.

The bow of the wafers coated on one side only changed by 1.1–1.3 μm, corresponding to an average stress of ~ 300 MPa. For the wafers coated on both sides the change in bow was limited to 0.2–0.6 μm, an improvement by a

factor of $\sim$ 2–5. Nevertheless, extrapolating these results to a glass sheet of half the thickness, twice the diameter, and half the elastic modulus one would still expect a change in bow of $\sim$ 6–19 μm, assuming the same thin film stress.

4.2. Sputtered Cr/Au films

Sputtering in principle allows control of stress in thin films. Fine-tuning of sputtering parameters such as sputtering gas pressure, flux, or substrate bias enables growing films under tensile or compressive stress. If films can therefore be sputter deposited with minimal stress, coating of wafers on both sides should allow for minimal changes in wafer bow.

We repeated the above experiment with sputtered films. The bow of all wafers was measured before coating. Sputtering was performed at Raytheon Lexington Labs. A number of small monitor wafers were sputtered with Cr/Au films of the same nominal thicknesses as the evaporated films, their stresses were measured, and the sputtering parameters were varied in an attempt to find parameters that minimize stress before coating the sample wafers. Three wafers were coated on one side only, and three were coated on both sides. Five sputtering runs were performed with nominally identical parameters, with two wafers at a time. From the $\sim$ 0.4 μm change in bow of the wafers that were coated on one side only one can deduce an average stress of $\sim$ 100 MPa. For the double-sided coated wafers the changes in bow were $-0.091 \pm 0.080\mu$m, $-0.030 \pm 0.030\mu$m, and $+0.28 \pm 0.08\mu$m. The first two wafers (nos. 1 and 2) were coated in subsequent sputtering runs, while the third wafer had its two sides coated before and after wafers 1 and 2. Its relatively large change in bow might be due to insufficient control of sputtering conditions between the two depositions. However, the change in bow for wafers 1 and 2 is close to the measurement resolution. Thus it is possible to balance thin-film stress-based deformation of thin substrates through deposition of similar films on both sides.

The results on Si wafers can only give order-of-magnitude estimates for the behavior of glass sheets covered with the same layer structure. The stress in these reflective films depends to some degree on the structure of the substrate (amorphous glass vs. crystalline Si) and its coefficient of thermal expansion (7.2×10^{-6} K^{-1} for D-263 vs. 2.6×10^{-6} K^{-1} for Si). Once our UV Shack-Hartmann wavefront sensor[21] is in operation we therefore will persue further studies on glass sheet deformation under thin-film stress.

It should also be mentioned that due to the tightly stacked arrangements at small grazing angles it might not be desirable to have a highly reflective coating on the back of a thin-foil optic. In this case stress-induced bowing could still be reduced by deposition of a low-reflectivity film on the back side that is stress-matched to the reflective film on the front of the optic.

5. DISCUSSION

We have investigated novel methods for the shaping of flat thin-foil optics and obtained encouraging results from slumping to TiO_2 coated pin chucks. A number of improvements can be made to the current pin chucks. The pin shape and size can be better controlled through the use of directional plasma etching instead of the isotropic wet HF etch employed so far. This will allow for taller pins of smaller cross sectional area, which should prevent deformation from larger dust particles and reduce the contact area between glass and mandrel even further. Unfortunately, the rough, non-sticking TiO_2 coating has proven to be difficult to reproduce reliably. We are therefore also investigating alternative methods to roughen the top of the pins.

The sizes of our slumped glass sheets to date are relatively small. Experiments on larger mandrels and microsheets are in order, which require a larger oven. The suppression of edge effects also needs to be improved. Nevertheless, we believe that the shaping of microsheets to flat mandrels can be improved through careful design of the mandrel surface, and scaled up in size in a well temperature-controlled environment.

Despite physical contact with the mandrel surface, slumping the reflecting side of a microsheet to a precisely shaped mandrel has the advantage that the reflecting side is close to the ideal shape, while glass thickness variations will mainly affect the figure on the back of the foil.

Flat foils are far more susceptible to bending than comparable small radius-of-curvature cylindrical or conical foils along the axial direction.[17] Thin-film stress should therefore be avoided or compensated for as much as possible to avoid overconstraining mounts. High-accuracy foil assembly schemes with $\sim$ 0.5 μm accuracy are easier to implement when small or no foil distortion is required for mounting.[6] Replicating a blazed grating with UV curable epoxy can

in principle contribute to bimaterial bending, but for the Constellation-X design the epoxy layer could be as thin as 26 nm,[10] compared to the tens of microns often necessary in epoxy replicated foils for Wolter-type mirrors. Any remaining predictable bending can then in principle be mitigated through a properly designed low-reflection coating on the back of the foil.

Shaping foils to flat mandrels has certain advantages over curved geometries. It is easier to shape and polish flat mandrels to higher precision. And at some level shaping and alignment will be limited by the available metrology, which is simpler, more precise, and less expensive for flat - or in the case of KB optics, nearly flat - optics.

The proposed manufacturing of many flat, large-area foil-optic reflection gratings consists of thermal shaping of microsheets, UV curable epoxy grating replication from a high-efficiency Si master, and low-stress two-sided coating. An alternative method under investigation by the authors that eliminates the grating replication step would be the flattening of Si wafers, followed by direct lithographic manufacture of the grating on each wafer, and final coating similar to the case of glass. Both methods promise significant weight reduction and highly efficient grating diffraction at reasonable cost.

6. SUMMARY

Novel methods for the shaping of flat thin-foil x-ray optics have been investigated. Away from the edges of 50×50 mm^2 microsheets we achieved rms angular deviations as low as 10 arc seconds and HPD of ~ 6 arc seconds with a lithographically defined pin chuck that serves as the slumping mandrel. This approach circumvents the need for epoxy replication from superpolished mandrels and offers a low-cost alternative for the production of flat light-weight mirrors and high-efficiency reflection gratings. Microscopic control of the shaping surface and good temperature uniformity should allow forming of large-area microsheets to the arc second level. For sub-micron accuracy mounting schemes foil distortions should be kept to a minimum, which can be achieved through double-sided coatings tailored to the needs and geometries of x-ray telescope optics.

ACKNOWLEDGMENTS

We gratefully acknowledge excellent technical support from E. Murphy (Space Nanotechnology Lab, SNL), R. Fleming (SNL), W. Gu (SNL), J. Daley (Nanostructures Lab, NSL), E. Moon (NSL), J. Carter (NSL), T. McClure (Center for Materials Science and Engineering), P. W. O'Brien (MIT Lincoln Lab), J. K. Rawson (Raytheon), P. Cremin (Raytheon), and facility and staff support from the Microsystems Technology Lab at MIT. This work was supported by the National Aeronautics and Space Administration (NASA) under grants NAG-5271, NAS5-98037, and NCC5-525.

REFERENCES

1. M. C. Weisskopf, "Chandra X-ray Observatory: a review of the performance of the optics," in *X-Ray Optics for Astronomy: Telescopes, Multilayers, Spectrometers, and Missions"*, *Proc. SPIE* **4496** (these proceedings).
2. H. Tananbaum, "Chandra overview," in *X-ray Astronomy 2000*, R. Giacconi, S. Serio, and L. Stella, eds., *ASP Conf. Proc.* **CS-234**, Oct. 2001.
3. C. J. Hailey, S. Abdali, F. E. Christensen, W. W. Craig, T. R. Decker, F. A. Harrison, and M. Jimenez-Garate, "Substrates and mounting techniques for the High-Energy Focusing Telescope (HEFT)," in *EUV, X-Ray, and Gamma-Ray Instrumentation for Astronomy VIII*, O. H. Siegmund and M. A. Gummin, eds., *Proc. SPIE* **3114**, pp. 535–543, 1997.
4. W. W. Craig, F. E. Christensen, T. A. Decker, C. J. Hailey, F. A. Harrison, R. M. Hill, M. A. Jimenez-Garate, P. H. Mao, and S. M. Schindler, "Hard x-ray optics for the HEFT balloon-borne payload: prototype design and status," in *EUV, X-Ray, and Gamma-Ray Instrumentation for Astronomy IX*, O. H. Siegmund and M. A. Gummin, eds., *Proc. SPIE* **3445**, pp. 112–120, 1998.
5. R. Petre, C. G. Chen, L. M. Cohen, D. A. Content, R. J. Harms, O. Mongrard, G. P. Monnelly, T. T. Saha, M. L. Schattenburg, P. J. Serlemitsos, and W. W. Zhang, "Segmented x-ray mirror development for Constellation-X," in *X-Ray Optics, Instruments, and Missions II*, R. B. Hoover and A. B. Walker, eds., *Proc. SPIE* **3766**, pp. 11–21, 1999.
6. G. P. Monnelly, O. Mongrard, D. Breslau, N. Butler, C. G. Chen, L. Cohen, W. Gu, R. K. Heilmann, P. T. Konkola, G. R. Ricker, and M. L. Schattenburg, "High-accuracy x-ray foil optic assembly," in *X-Ray Optics, Instruments, and Missions IV*, R. B. Hoover and A. B. Walker, eds., *Proc. SPIE* **4138**, pp. 164-173, 2000.

7. W. W. Craig, C. J. Hailey, M. A. Jimenez-Garate, and D. L. Windt, "Development of thermally formed glass optics for astronomical hard x-ray telescopes," *Optics Express* **7**, pp. 178–185, 2000.
8. R. Petre, L. M. Cohen, D. A. Content, J. Hein, T. T. Saha, M. L. Schattenburg, and W. W. Zhang, "Progress toward meeting the Constellation-X performance goals using segmented x-ray mirrors," in *X-Ray Optics, Instruments, and Missions IV*, R. B. Hoover and A. B. Walker, eds., *Proc. SPIE* **4138**, pp. 16-24, 2000.
9. H. D. Tananbaum, N. E. White, J. A. Bookbinder, F. E. Marshall, F. A. Cordova, "Constellation X-ray mission: implementation concept and science overview," in *EUV, X-Ray, and Gamma-Ray Instrumentation for Astronomy X*, O. H. Siegmund and K. A. Flanagan, eds., *Proc. SPIE* **3765**, pp. 62–72, 1999.
10. S. M. Kahn, F. B. Paerels, J. R. Peterson, A. P. Rasmussen, M. L. Schattenburg, G. R. Ricker, Jr., M. W. Bautz, J. P. Doty, G. Y. Prigozhin, J. A. Nousek, D. N. Burrows, J. E. Hill, and W. C. Cash, "Large-area reflection grating spectrometer for the Constellation-X mission," in *EUV, X-ray, and Gamma-ray Instrumentation in Astronomy X*, O. H. Siegmund and K. A. Flanagan, eds., *Proc. SPIE* **3765**, pp. 94–103, 1999.
11. P. Kirkpatrick and A. V. Baez, "Formation of optical images by x-rays," *J. Opt. Soc. Amer.* **38**, pp. 766-774, 1948.
12. A. E. Franke, M. L. Schattenburg, E. M. Gullikson, J. Cottam, S. M. Kahn, and A. Rasmussen, "Super-smooth x-ray reflection grating fabrication," *J. Vac. Sci. Technol. B* **15**, pp. 2940–2945, 1997.
13. K. V. Ravi, "Wafer flatness requirements," in *Future Fab International*, Issue 7, pp. 207–212, Technology Publishing Ltd., London, 1999.
14. T. Bailey, B. J. Choi, M. Colburn, M. Meissl, S. Shaya, J. G. Ekerdt, S. V. Sreenivasan, and C. G. Willson, "Step and flash imprint lithography: Template surface treatment and defect analysis," *J. Vac. Sci. Technol. B* **18**, pp. 3572-3577, 2000.
15. I. Ghozeil, "Hartmann and other screen tests," in *Optical Shop Testing*, D. Malacara, ed., pp. 376–396, Wiley-Interscience, New York, 1992.
16. W. Kern, in *Handbook of Semiconductor Wafer Cleaning Technology*, W. Kern, ed., Noyes Publications, New Jersey, 1993.
17. M. A. Jimenez-Garate, W. W. Craig, C. J. Hailey, F. E. Christensen, and A. Hussain, "Fabrication, performance, and figure metrology of epoxy-replicated aluminum foils for hard x-ray focusing multilayer-coated segmented conical optics," *Opt. Eng.* **39**, pp. 2982-2994, 2000.
18. M. A. Jimenez-Garate, "The development of hard x-ray telescope optics and a theoretical model of x-ray emission from accretion disks," Ph.D. thesis, Columbia University, 2001.
19. F. E. Christensen, W. W. Craig, D. L. Windt, M. A. Jimenez-Garate, C. J. Hailey, F. A. Harrison, P. H. Mao, J. M. Chakan, E. Ziegler, V. Honkimaki, "Measured reflectance of graded multilayer mirrors designed for astronomical hard X-ray telescopes," *Nucl. Instrum. Meth. A*, **451**, pp. 572–581, 2000.
20. C. G. Chen, L. M. Cohen, R. K. Heilmann, P. T. Konkola, O. Mongrard, G. P. Monnelly, and M. L. Schattenburg "Micro-Comb Design and Fabrication for High Accuracy Optical Assembly," *J. Vac. Sci. Technol. B* **18**, pp. 3272–3276, 2000.
21. M. McGuirk, G. P. Monnelly, M. L. Schattenburg, C. R. Canizares, and C. G. Witthoft, "Wavefront sensors for x-ray and EUV optics fabrication", in *X-Ray Optics for Astronomy: Telescopes, Multilayers, Spectrometers, and Missions"*, *Proc. SPIE* **4496** (these proceedings).
22. G. G. Stoney, "The tension of metallic films deposited by electrolysis," *Proc. R. Soc. London Ser. A* **82**, pp. 172-175, 1909.
23. O. Mongrard, "High accuracy foil optics for x-ray astronomy," Master's thesis, MIT, 2001.